

## **Without human-caused climate change temperatures of 40°C in the UK would have been extremely unlikely**

Mariam Zachariah<sup>1</sup>, Robert Vautard<sup>2</sup>, Dominik L. Schumacher<sup>3</sup>, Maja Vahlberg<sup>4</sup>, Dorothy Heinrich<sup>4</sup>, Emmanuel Raju<sup>5</sup>, Lisa Thalheimer<sup>6,7</sup>, Julie Arrighi<sup>4,8,9</sup>, Roop Singh<sup>4</sup>, Sihan Li<sup>7</sup>, Jingru Sun<sup>10</sup>, Gabriel Vecchi<sup>10,11</sup>, Wenchang Yang<sup>10</sup>, Sonia I. Seneviratne<sup>3</sup>, Simon F. B. Tett<sup>12</sup>, Luke J. Harrington<sup>13</sup>, Piotr Wolski<sup>14</sup>, Fraser C. Lott<sup>15</sup>, Mark McCarthy<sup>15</sup>, Jordis S. Tradosky<sup>16,17</sup>, Friederike E. L. Otto<sup>1</sup>

1 Grantham Institute, Imperial College London, UK

2 Institut Pierre-Simon Laplace, CNRS, Sorbonne Université, Paris, France

3 Institute for Atmospheric and Climate Science, Department of Environmental Systems Science, ETH Zurich, Zurich, Switzerland

4 Red Cross Red Crescent Climate Centre, The Hague, the Netherlands

5 Department of Public Health, Global Health Section & Copenhagen Centre for Disaster Research, University of Copenhagen, Denmark

6 Princeton School of Public and International Affairs, Princeton University, Princeton, NJ 08540, USA.

7 School of Geography and the Environment, University of Oxford, UK

8 Faculty of Geo-Information Science and Earth Observation (ITC), University of Twente, Enschede, the Netherlands

9 Global Disaster Preparedness Center, American Red Cross, Washington DC, USA

10 Department of Geosciences, Princeton University, Princeton, NJ 08544, USA

11 High Meadows Environmental Institute, Princeton University, Princeton, NJ 08540, USA

12 School of Geosciences, University of Edinburgh, Edinburgh, UK

13 Te Aka Mātuatua School of Science, University of Waikato, Hamilton 3216, New Zealand

14 Climate System Analysis Group, University of Cape Town

15 Met Office Hadley Centre, Exeter EX1 3PB, UK

16 Deutscher Wetterdienst (DWD), Regionales Klimabüro Potsdam, Potsdam, Germany

17 Bodeker Scientific, Alexandra, New Zealand

## **Main findings**

- The 2022 heatwave is estimated to have led to at least 13 deaths from drowning, it brought challenging conditions for the NHS with a spike in emergency calls, and care services

supporting the elderly and vulnerable were put under increased stress, with a likely increase in heat related deaths. The impacts were unequally distributed across demographics. Even within London, there are high levels of inequity in experienced temperatures, with certain, often poorer neighbourhoods, lacking green space, shade, and water which can be lifelines during heatwave.

- While Europe experiences heatwaves increasingly frequently over the last years, the recently observed heat in the UK has been so extreme that it is also a rare event in today's climate. The observed temperatures averaged over 2 days were estimated to have a return period of approx. 100 years in the current climate. For the 1-day maximum temperatures over the region shown in Fig. 1 the return time is estimated at 1 in 1000 years in the current climate. Note that return periods of temperatures vary between different measures and locations, and are therefore highly uncertain.
- At three individual stations the 1-day maximum temperatures are as rare as 1 in 500 years in St James Park in London, about 1 in 1000 years in Durham and only expected on average once in 1500 years in today's climate in Cranwell, Lincolnshire.
- The likelihood of observing such an event in a 1.2C cooler world is extremely low, and statistically impossible in two out of the three analysed stations.
- The observational analysis shows that a UK heatwave as defined above would be about 4C cooler in preindustrial times.
- To estimate how much of these observed changes is attributable to human-caused climate change we combine climate models with the observations. It is important to highlight that all models systematically underestimate the observed trends. The combined results are thus almost certainly too conservative.
- Combining the results based on observational and model analysis, we find that, for both event definitions, human-caused climate change made the event at least 10 times more likely. In the models, the same event would be about 2C less hot in a 1.2C cooler world, which is a much smaller change in intensity than observed.
- This discrepancies between the modelled and observed trends and variability also hinders confidence in projections of the future trends.
- Heatwaves during the height of summer pose a substantial risk to human health and are potentially lethal. This risk is aggravated by climate change, but also by other factors such as an ageing population, urbanisation, changing social structures, and levels of preparedness. The full impact is only known after a few weeks when the mortality figures have been analysed. Effective heat emergency plans, together with accurate weather forecasts such as those issued before this heatwave, reduce impacts and are becoming even more important in light of the rising risks.

## 1 Introduction

On Monday and Tuesday, the 18th & 19th of July, an exceptional heat wave affected large parts of the UK. It was the first time that temperatures of 40°C and above have been forecast in the UK. On Tuesday, 40.3°C was reached in Coningsby in Lincolnshire, breaking the previous maximum temperature record of 38.7°C, which was reached at Cambridge Botanic Garden on 25 July 2019, by 1.6C. In total 46 stations met or exceeded the previous record in a band stretching from Kent to north Yorkshire, and a temperature above 35°C was recorded in Scotland for the first time breaking the previous record of 32.9°C from 9 August 2003. Minimum temperatures were also extremely high with 25.8°C provisionally being recorded in Kenley in Surrey, breaking the previous record from 1990 by 1.9°C.

The heatwave was very well forecast, and the UK Met Office issued severe weather warnings well ahead of the heat. A Level 4 UK Health Security Agency [Heat Health Alert](#) had been issued for Monday and Tuesday. This alert level is used when a heatwave is so severe and/or prolonged that its effects extend outside the health and social care system. At this level, illness may occur among the fit and healthy, and not just in high-risk groups.

The heatwave in the UK occurred as part of a large Western European heat wave generated by high pressure over Central and Western Europe and very warm air flowing in from North Africa. While the heat was only very extreme for the two days of the 18th & 19th of July in the UK, other parts of Western and Southern Europe experienced more prolonged heat.

The heatwave event was also very dry and followed a longer dry spell in the UK, reaching back to November 2021<sup>1</sup>. In terms of rainfall, July 2022 was the UK's driest since 1911<sup>1</sup>. Drought conditions have also been widespread across continental Europe in recent months (Figure S1). Given the higher background temperatures, it can also be expected that evapotranspiration was higher, and thus that soil moisture was particularly low ([Seneviratne et al. 2021](#)). Dry soil moisture conditions can further enhance the temperature of heatwaves substantially ([Seneviratne et al. 2010](#), [Miralles et al. 2014](#), [Wehrli et al. 2019](#)), a mechanism that is very likely to have played a role in this event.

Whilst full after-event reports of the heatwaves impacts are yet to be completed, impacts include projections of excess mortality, hospitalisations, and psychosocial effects. The heatwave also caused fires throughout London; public transport was significantly impacted with trains cancelled due to damage to the tracks and risks to the wires; and many IT systems, particularly in hospitals, failed due to power outages. Whilst full after-event reports of the heatwaves impacts are yet to be completed, impacts include projections of excess mortality of over 840 people for the 18th and 19th of July, hospitalisations, infrastructure damage, and psychosocial effects. Vulnerability and exposure dynamics which turned this extreme weather into impacts include the unprecedented nature of the event, preparedness, early warning, and response, unadapted infrastructure and urban planning, and differential impacts on certain groups and demographics.

---

<sup>1</sup> <https://blog.metoffice.gov.uk/2022/07/27/july-2022-a-dry-run-for-uks-future-climate/>

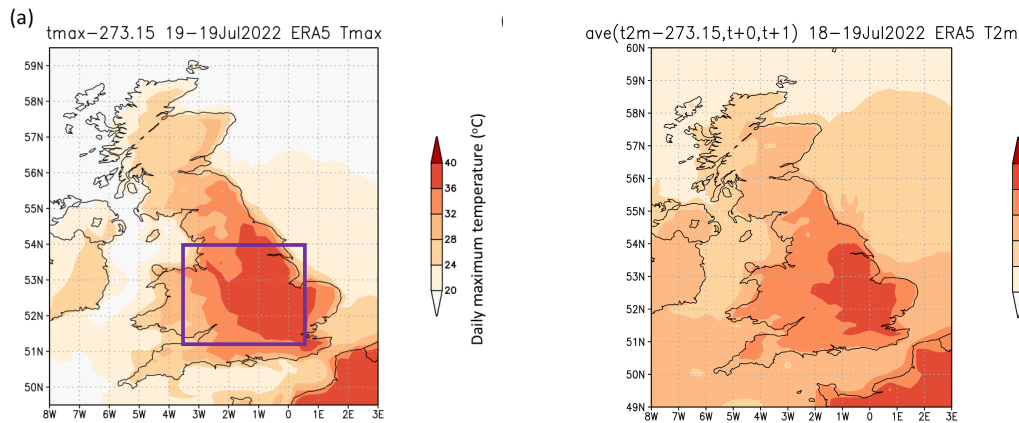


Figure 1: ERA5 near surface temperature ( $T2m$ ) [ $^{\circ}C$ ] for a) the 19th of July 2022 showing daily maximum and b) the 2-day average over the 18th & 19th of July 2022. The rectangle represents the study region at 51.25-54  $^{\circ}N$ , 3.5W-0.5  $^{\circ}E$ .

To investigate the extent to which human-caused climate change altered the frequency of occurrence of the extremely high temperatures, across the region affected by the most extreme heat (see Figure 1), we choose to analyse the 2-m temperature over land in the region 51.25-54  $^{\circ}N$ , 3.5W-0.5  $^{\circ}E$  (highlighted by magenta box in Fig. 1). This region covers the [area of the red alert warning issued by the Met Office](#), including London, and the station where the daily maximum UK temperature record was broken on the 19th of July 2022. To account for the event itself, which lasted two days and nights, as well as for the record breaking temperature, we decided to use two event definitions, i.e. we analyse the annual maximum of 2-day average temperatures over this region as well as the annual maximum of the daily maximum temperature (TXx). Additionally, we analyse the change in frequency and intensity of the maximum observed daily temperature of 2022 at 3 locations: London's St James Park, Cranwell in Lincolnshire which is geographically close to Coningsby, where the new UK record has been set, but has a longer observed time series, and Durham, which although is located outside the red alert area, has a very long record going back to 1880 and also experienced very high temperatures given its latitude of  $\sim 54.78$  North. Temperatures at Durham were 36.9 $^{\circ}C$ , breaking the previous record by 4 $^{\circ}C$ .

In most parts of the world there is very high confidence that the duration, intensity and likelihood of extreme heat has increased dramatically due to human-induced climate change (Seneviratne et al. 2021). This is particularly also the case in Europe, including the UK. The first event attribution study related to the European heatwave of 2003 (Stott et al 2004), and more recently, the joint UK temperature record set during the 2018 heatwave was found to be 30 times more likely due to human activity (McCarthy et al 2019). Following another new UK record in 2019, Christidis et al 2020 examined the return time for a 40 $^{\circ}C$  day anywhere in the UK (at that time purely theoretical). It was found to be between 100 and 300 years in the present, up from 100 to 1000s without human influence. The IPCC AR6 assessment concludes with extremely high confidence (very likely) an increase in the intensity and frequency of hot extremes in the region, as well as a high confidence in a human contribution to the observed increase in the intensity and frequency of hot extremes (Seneviratne et al. 2021; see in particular Table 11.7 in that chapter). The assessment presented there is based on several lines of evidence: physical understanding; observations of an increase in hot extremes and heat waves with respect to frequency, intensity and duration; climate model simulations of changes in heat extremes under different levels of warming and attribution studies of individual heat waves as well as

of global hot extremes. These lines of evidence mean that globally, as a direct result of climate change, previously very rare heat is now just unusual (Donat *et al* [2016](#), King [2017](#), Dunn *et al* [2020](#), Seong *et al* [2021](#)). While, in some cases, events now considered 'extreme' reach temperatures that were formerly all but impossible (Rahmstorf and Coumou [2011](#), Imada *et al* [2019](#), Sippel *et al* [2020](#), Robinson *et al* [2021](#)).

Long-term changes in heatwaves are influenced not only by globally well-mixed greenhouse gases but also by more localised influences, including aerosol trends (P  r   et al., [2011](#)), land use changes (Cowan, Hegerl, et al., [2020](#)), vegetation and soil moisture changes (Seneviratne et al. [2010](#), Donat et al., [2017](#)), irrigation (Thiery et al., [2017](#)), and urbanisation effects (Heaviside et al., [2017](#)). Furthermore, the meteorological conditions conducive to heatwaves could change regionally by potential changes in mean atmospheric circulation or in the frequency of specific weather patterns leading to extreme heat (Horton et al., [2015](#)).

Heatwaves, on the scales people experience them, are strongly influenced by the local energy budget that determines the use of energy between evaporation and heating, set by the land surface, vegetation, irrigation, and urbanisation. Other factors such as circulation changes or aerosols may also be important and feedbacks may well be misrepresented in climate models during these extreme circumstances (Vogel et al. [2018](#)). Many of these drivers and feedbacks are not well-simulated in current climate models as evidenced by striking discrepancies between observed and modelled trends and variability in certain regions of the globe. Van Oldenborgh et al. ([2022](#)) show that the discrepancies cannot always be explained by natural variability and in some cases are well outside the range of CMIP historical simulations even in well-understood regions (Cowan, Undorf, et al., [2020](#); van Oldenborgh et al., [2018](#)).

## **2 Data and methods**

### **2.1 Observational data**

The primary dataset used in this study for characterising the heatwave is the ERA5 reanalysis (Hersbach et al., [2020](#)), extended to the time of the heatwave by ECMWF operational analyses produced using a later version of the same model. All fields were downloaded at 0.25  resolution from ECMWF. Both products are optimal combinations of observations, including near-surface temperature observations from meteorological stations, and the high-resolution ECMWF weather forecast model-Integrated Forecasting System (IFS). Due to the constraints of the surface temperature observations, we expect no large biases between the main dataset and the extension, although some differences may be possible under these extreme conditions.

Observed records of daily maximum temperature for 3 stations: St James Park, Durham and Cranwell were made available for this study by the UK Met Office. These datasets span 1944-2022, 1880-2022 and 1978-2022, respectively. They are used in this study as an additional line of evidence.

As a measure of anthropogenic climate change we use the (low-pass filtered) global mean surface temperature (GMST), where GMST is taken from the National Aeronautics and Space Administration (NASA) Goddard Institute for Space Science (GISS) surface temperature analysis (GISTEMP, [Hansen et al., 2010](#) and [Lenssen et al. 2019](#)).

### **2.2 Model and experiment descriptions**

We use five multi-model ensembles from climate modelling experiments using very different framings ([Philip et al., 2020](#)): Sea Surface temperature (SST) driven global circulation high resolution models, coupled global circulation models and regional climate models.

The first model ensemble is the Coordinated Regional Climate Downscaling Experiment- European Domain (EURO-CORDEX) with 0.11° resolution (WAS-22) ([Jacob et al., 2014](#); [Vautard et al., 2021](#)). The ensemble (see Table 2) consists of 11 regional climate models each of which are driven by 8 GCMs.

The second ensemble includes the AM2.5C360 ([Yang et al. 2021](#), [Chan et al. 2021](#)) and the FLOR ([Vecchi et al. 2014](#)) climate models developed at Geophysical Fluid Dynamics Laboratory (GFDL). The AM2.5C360 is an atmospheric GCM based on that in the FLOR model ([Delworth et al. 2012](#), [Vecchi et al. 2014](#)) with a horizontal resolution of 25 km. Ten ensemble simulations of the Atmospheric Model Intercomparison Project (AMIP) experiment (1871-2021) are analysed. These simulations are initialised from ten different pre-industrial conditions but forced by the same SSTs from HadISST1 ([Rayner et al. 2003](#)) after groupwise adjustments ([Chan et al. 2021](#)), as well as the same historical radiative forcings. The FLOR model, on the other hand, is an atmosphere-ocean coupled GCM with a resolution of 50 km for land and atmosphere and 1 degree for ocean and ice. Five ensemble simulations from FLOR are analysed, which cover the period from 1860 to 2100 and include both the historical and RCP4.5 experiments driven by transient radiative forcings from CMIP5 ([Taylor et al. 2012](#)).

We also examined a multitude of CMIP6 simulations ([Eyring et al., 2016](#)). For all simulations, the period 1850 to 2015 is based on historical simulations, while the SSP5-8.5 scenario is used for the remainder of the 21st century. Models are excluded if they do not provide all relevant variables, do not cover 1850–2100, or include duplicate time steps or missing time steps. All available ensemble members are used. These criteria are fulfilled and the validation tests for the 2-day average daily mean temperature (Section 4) are passed by a total of 8 models (29 ensemble members).

The fourth ensemble considered in this study is the HighResMIP SST-forced model ensemble ([Haarsma et al. 2016](#)), the simulations for which span from 1950 to 2050. The SST and sea ice forcings for the period 1950-2014 are obtained from the 0.25° x 0.25° Hadley Centre Global Sea Ice and Sea Surface Temperature dataset that have undergone area-weighted regridding to match the climate model resolution (see Table B). For the ‘future’ time period (2015-2050), SST/sea-ice data are derived from RCP8.5 (CMIP5) data, and combined with greenhouse gas forcings from SSP5-8.5 (CMIP6) simulations (see Section 3.3 of Haarsma et al. 2016 for further details).

The fifth ensemble used is a pair of 525 member atmospheric model ensembles of HadGEM3-GA6-N216 with a resolution of about 60km ([Ciavarella et al., 2018](#)). One driven with HadISST1 SSTs and Sea-ice, and anthropogenic and natural forcings. A second driven with naturalised SSTs and Sea-ice, and natural forcings. These ensembles are available from 2016 to 2021 (inclusive). Estimation of the anthropogenic contribution to changes in intensity and probability of extreme events was computed using pooled data from the two ensembles.

The 1950-2022 period for which the observed data (ERA5) is available is chosen for model evaluation, while the entire length of simulations upto the year 2022 is considered for the attribution analysis. For the SST-forced simulations, we used observed GMST as covariate whereas the coupled models use the model GMSTs..

In this study, we follow the multi-method multi-model attribution that uses observations and climate model runs for making attribution assessments. Methods for observational and model analysis and for model evaluation and synthesis are used according to the World Weather Attribution Protocol, described in [Philip et al. \(2020\)](#), with supporting details found in [van Oldenborgh et al. \(2021\)](#), [Ciavarella et al. \(2021\)](#) and on the [World Weather Attribution website](#)<sup>2</sup>. The analysis steps include: (i) trend calculation from observations; (ii) model validation; (iii) multi-method multi-model attribution and (iv) synthesis of the attribution statement.

### 2.3 Statistical methods

In this approach, we calculate the return period, Probability Ratio (PR; the factor-change in the event's probability) and change in intensity of the event in order to compare the climate of today and the climate of the past, defined respectively by the GMST values of 2022 and the pre-industrial past (1850-1900, based on the Global Warming Index<sup>3</sup>). The difference in GMST between these two climates is currently 1.2 °C. This approach is followed for both observations and the models with transient runs. While the CMIP6 data are analysed using the same statistical models as the main method, the parameter uncertainty is estimated in a Bayesian setting using a Markov Chain Monte Carlo (MCMC) sampler instead of a bootstrapping approach (see [Ciavarella et al. 2021](#) for details).

To statistically model the event under study, we use a Generalized Extreme Value (GEV) distribution that shifts with GMST. The shape parameter of the GEV distribution is almost always found to be negative in heatwave analyses, resulting in the distribution having an upper bound (Wehner et al., 2018). This shape of the tail implies that the probability of an event to occur decreases rapidly as the upper bound is approached and is zero above it. We are not aware of a rigorous derivation of the origin of the upper bound in the literature. We think it could be a consequence of the nonlinearities in the surface energy balance and its interaction with the water balance, plus convection as a moderating effect. Both the sensible and latent heat fluxes increase rapidly with temperature. The assumption of constant scale and shape parameters in the distribution implies that the upper bound shifts with the rest of the distribution, which is found in observations as well as historical model simulations (Vautard et al., 2020).

In addition to the transient data analysis, we use simulations from two model experiments, one for current conditions and one for a counterfactual world without climate change that keeps CO<sub>2</sub> and other anthropogenic greenhouse gases fixed at pre-industrial levels. The probability ratio in this case, is estimated from the probabilities of the event from the factual and counterfactual forcing experiments. The uncertainties in this case are calculated from many bootstrap samples with percentile sampling ([Undorf et al., 2020](#)).

The threshold value for all of these models is estimated against the return period in the current climate, based on the observed dataset. Thereafter, the return period in the counterfactual scenario is also calculated against this threshold. The probability ratio is simply the ratio of the two probabilities (or return periods). The same procedure is used for the estimation of change in intensity of the event,  $\Delta I$ . Finally, results from observations and the models that pass the validation tests are synthesized into a single attribution statement.

---

<sup>2</sup> <https://www.worldweatherattribution.org/pathways-and-pitfalls-in-extreme-event-attribution>

<sup>3</sup> <https://www.globalwarmingindex.org>

### 3 Observational analysis: return time and trend

#### 3.1 Analysis of point station data

Although the attribution analysis in this study is performed with gridded data for events that are defined as regional averages, as an additional line of evidence, we also analyse the trends in annual maxima of daily maximum temperatures at 3 locations where peak temperatures were reported during the event, and estimate the return period of the 2022 records in the current and a 1.2 °C cooler climates. Fig. 2 shows the time series of annual maxima at 3 stations- StJames's Park (Fig. 2(a)), Durham (Fig. 2(b)) and Cranwell (Fig. 2(c)). All stations show increasing trends for this period, consistent with global warming signals observed for Central England temperatures (CET; [Károly and Stott, 2006](#)).

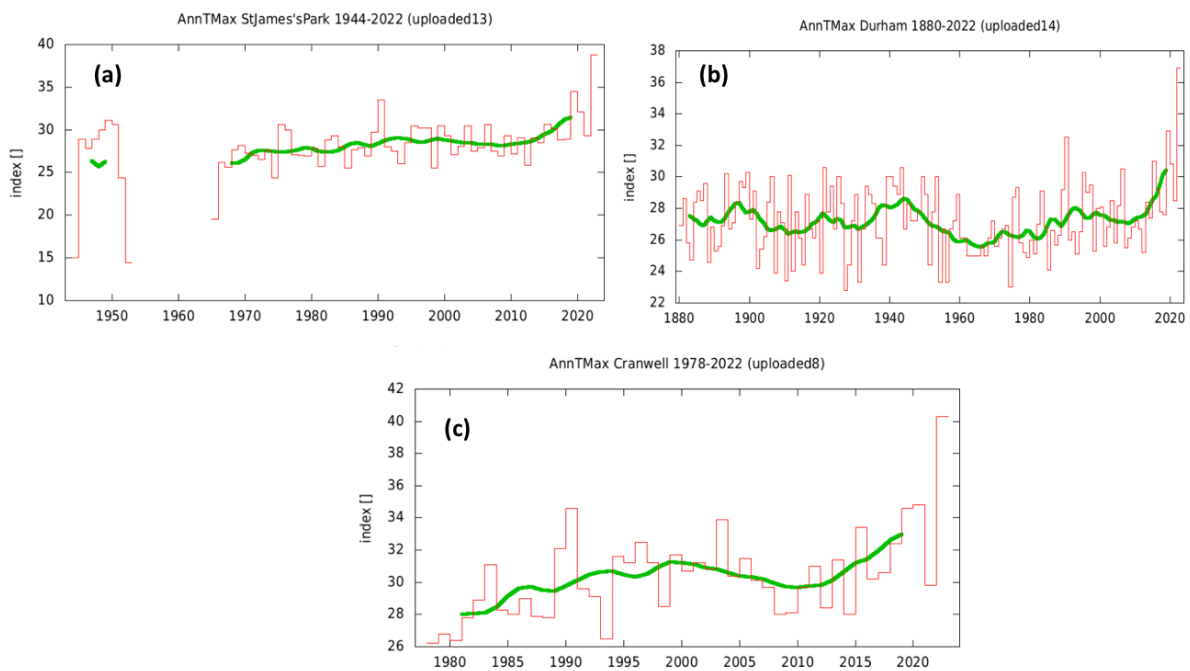


Fig. 2 Time series of annual maxima of daily maximum temperature along with the ten-year running mean (shown by the green line) for (a) St James's Park (b) Durham and (c) Cranwell.

Fig. 3 shows the trend fitting methods described in [Philip et al. \(2020\)](#) applied to the annual maxima of daily maximum temperature, for these three stations. The behaviour of the location parameter with respect to the GMST (panels a,c,e in Fig. 3) is found to increase with GMST. At St James's Park and Durham, the chances of observing 2022 values are only possible, when the possibility of the event occurring is included in the fit; Fig. A(b, d)). At Cranwell, such temperatures are still extremely rare, with a return time of 1600 years when the event is not included in the fit (Fig. 3(f)). By including the 2022 event in the fit, the return times of the 2022 event, although rare, are found to be significantly reduced- 590, 1100 and 150 years, respectively, for the three stations (not shown).

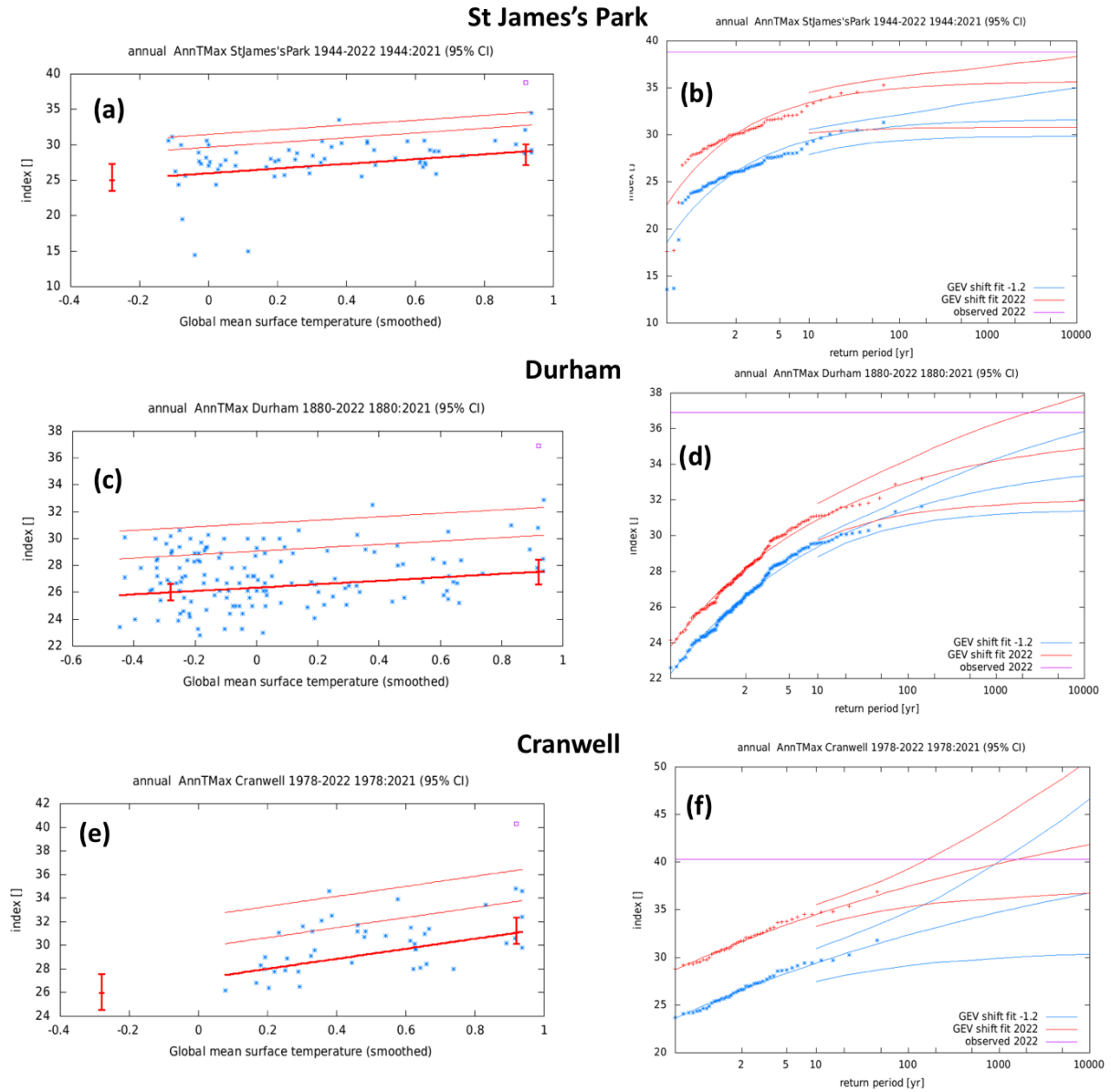


Fig. 3: Observational analysis at three locations, i.e. St. James Park London (top), Durham (middle), Cranwell (bottom). Left: the observed annual maximum temperature (TXx) as a function of the smoothed GMST anomaly. The thick red line traces the location parameter with time, while the thin red lines corresponds to the location parameters for the 6 and 40-yr return times. The July 2022 observation is highlighted with the magenta box. Right: Return time plots for the climate of 2022 (red) and a climate with GMST anomaly 1.2 °C cooler (blue). The past observations are shown twice: once scaled up to the current climate and once shifted down to the 1.2 °C cooler climate of the late nineteenth century. The magenta line shows the magnitude of the 2022 event analysed here.

### 3.2. Analysis of gridded data

Fig. 4 (a) shows the time-series of annual maxima of daily maximum temperature averaged over the study region, from 1950 to 2022. Fig. 4 (b) shows a similar plot for 2-day average daily mean temperature. Both series show steadily increasing trends for this period, consistent with global warming signals observed for Central England temperatures (CET; [Karoly and Stott, 2006](#)).

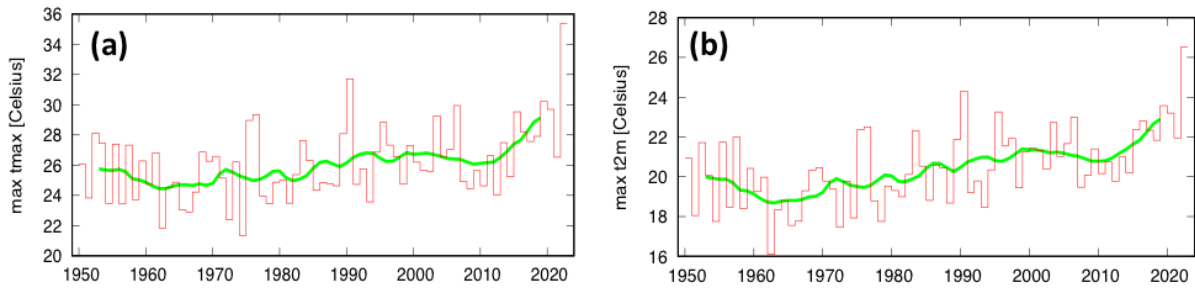


Fig. 4: Time series of area-averaged annual maxima of (a) daily maximum temperature along with the ten-year running mean (shown by the green line) and (b) 2-day average daily mean temperature, based on ERA5 dataset.

Fig. 5(a) shows the area-averaged annual maxima of daily maximum temperature as a function of the global mean surface temperature anomaly. The GEV-based return period curves for this variable in the present 2022 climate and the past climate when the global mean temperature was  $1.2^{\circ}\text{C}$  cooler are shown in Fig. 5(b). The best estimates for the return period of the 2022 event in the current climate emerges as a very rare 1-in-1000 year, and such an event would have been almost impossible in a world without climate change. Fig. 5(c-d) show similar plots for the area-averaged annual maxima of 2-day average daily temperature. Although the magnitude of the 2022 2-day event is still rare in the current climate with a return time of 100 years, such temperatures would also have been nearly impossible in the  $1.2^{\circ}\text{C}$  cooler climate of the past (Fig. 5(d)). For subsequent analysis, we use these return period estimates, i.e. 1-in-1000 years and 1-in-100 years for the 1-day maximum and 2-day averaged temperatures, respectively, to define the 2022 event.

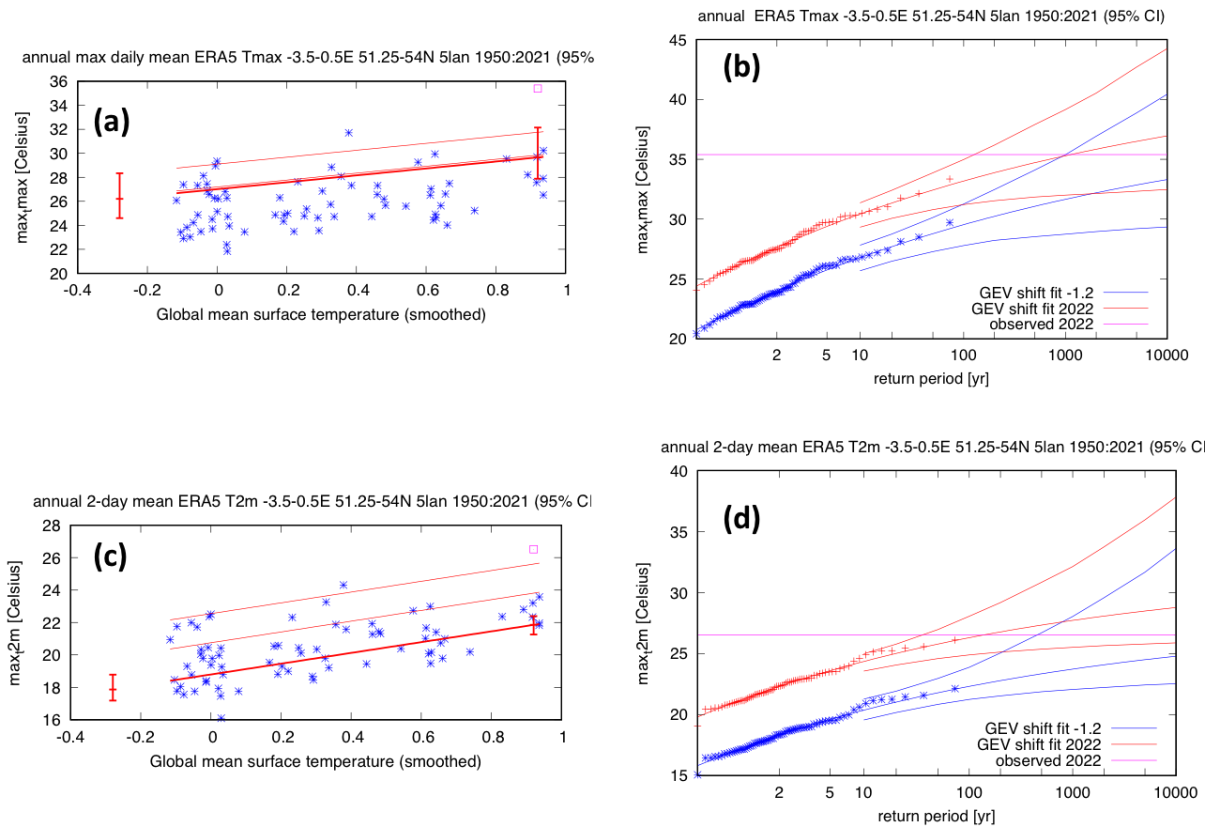


Fig. 5: (a) Response of annual maxima of daily maximum temperature averaged over the study region to change in global mean temperature. The thick red line denotes the time-varying mean, and the thin red lines show 1 standard deviation (s.d) and 2 s.d above. The vertical red lines show the 95% confidence interval for the location parameter, for the current, 2022 climate and the hypothetical, 1.2°C cooler climate. The 2022 observation is highlighted with the magenta box. (b) GEV-based return periods for the 2022 climate (red lines) and the 1.2°C cooler climate (blue lines with 95% CI). (c) same as (a) for annual maxima of 2-day average of daily mean temperature. (d) same as (b), for annual maxima of 2-day average of daily mean temperature.

#### 4 Model evaluation

Tables S1 and S2 show the results of model validation for the 1-day and 2-day event definitions, respectively. For the fixed SST runs, HadGEM-GA6-N216 uses the June-July maximum of the 1-day maximum and 2-day mean temperatures instead of annual maxima. However, this difference is not expected to alter the conclusions, as the highest temperatures in the UK mostly happen during these months. Because we have many models, we only use models with statistical parameters and uncertainty bounds within the respective ERA5-based bounds for the attribution analysis. These models are highlighted in green in the respective tables.

#### 5 Multi-method multi-model attribution

This section shows probability ratios and change in intensity ( $\Delta I$ ) in annual maximum of daily maximum temperature and annual maximum of 2-day average daily mean temperature in the study region, based on both observations and model simulations. Tables 1-2 show these values relative to

the present climate, for a past 1.2°C cooler climate and a future 2°C warmer world, respectively. It should be noted that only those models that passed the validation checks highlighted in green in Tables S1 and S2) are considered in this analysis.

**Table 1.** Probability ratio and change in intensity of the 2022 event described by annual maximum of daily maximum temperature when compared with a 1.2°C cooler climate, from the models that passed the validation tests.

Model / Observations	Probability ratio PR [-]	Change in intensity $\Delta I$ [°C]
ERA5	5.1e+2 (5.0 ... $\infty$ )	3.6 (1.9 ... 5.2)
CANESMr1-CCLM ()	6.6 (1.9 ... 1.0e+5)	2.1 (1.2 ... 3.2)
CANESMr1-REMO ()	25 (1.6 ... 1.0e+5)	1.1 (0.19 ... 1.9)
CNRMr1-CCLM ()	1.0e+5 (3.6 ... 1.0e+5)	2.1 (0.60 ... 3.6)
CNRMr1-COSMOcrCLIM ()	1.0e+5 (3.5 ... 1.0e+5)	1.5 (-0.010 ... 2.9)
CNRMr1-REMO ()	9.1e+2 (3.4 ... 1.0e+5)	2.9 (1.8 ... 4.2)
ECEARTHr12-COSMOcrCLIM ()	1.9 (0.88 ... 1.0e+5)	0.91 (-0.30 ... 2.1)
ECEARTHr12-HIRHAM ()	2.2 (0.072 ... 1.0e+5)	0.39 (-0.75 ... 1.8)
ECEARTHr12-REMO ()	3.2 (0.60 ... 1.0e+5)	0.89 (-0.55 ... 2.3)
ECEARTHr1-COSMOcrCLIM ()	2.3 (1.2 ... 2.1e+4)	1.3 (0.42 ... 2.3)
ECEARTHr1-HIRHAM ()	1.4e+3 (1.5 ... 1.0e+5)	1.2 (0.27 ... 2.3)
ECEARTHr3-COSMOcrCLIM ()	1.3 (0.72 ... 8.9)	0.46 (-0.57 ... 1.5)
ECEARTHr3-HIRHAM ()	8.6 (0.12 ... 1.0e+5)	0.58 (-0.52 ... 1.8)
ECEARTHr3-RCA ()	1.2 (0.043 ... 1.0e+5)	0.12 (-1.4 ... 2.1)
MIROCr1-CCLM ()	1.0e+5 (14 ... 1.0e+5)	2.5 (1.3 ... 3.8)
MPIr1-COSMOcrCLIM ()	32 (1.1 ... 1.0e+5)	1.0 (-0.24 ... 2.1)
MPIr1-HIRHAM ()	1.9e+9 (4.4 ... 1.0e+5)	2.0 (0.80 ... 3.3)
MPIr1-RCA ()	1.0e+5 (2.5 ... 1.0e+5)	2.5 (0.65 ... 4.2)
MPIr2-COSMOcrCLIM ()	1.3e+4 (0.52 ... 1.0e+5)	1.0 (-0.43 ... 2.3)
MPIr3-COSMOcrCLIM ()	82 (0.58 ... 1.0e+5)	0.96 (-0.62 ... 2.2)
NOESMr1-HADREM ()	84 (2.9 ... 1.0e+5)	3.0 (1.5 ... 4.7)
NOESMr1-HIRHAM ()	26 (0.66 ... 1.0e+5)	1.2 (-0.30 ... 2.8)
NOESMr1-RACMO ()	2.4e+2 (2.1 ... 1.0e+5)	1.7 (0.12 ... 3.3)
NOESMr1-RCA ()	4.0 (0.47 ... 1.0e+5)	1.3 (-1.0 ... 3.2)
NOESMr1-REGCM ()	2.8 (1.0 ... 1.0e+5)	2.4 (0.020 ... 4.3)
NOESMr1-REMO ()	3.0e+3 (2.2 ... 1.0e+5)	1.8 (0.49 ... 3.3)
NOESMr1-WRF381P ()	1.6 (0.93 ... 3.0e+3)	1.2 (-0.44 ... 2.6)
FLOR historical+RCP4.5 (5)	5.9e+4 (49 ... $\infty$ )	1.4 (1.2 ... 1.6)
AM2.5C360 amip (10)	22 (6.1 ... 6.4e+3)	1.4 (0.90 ... 1.8)
ACCESS-CM2 ssp585 (4)	39 (5.2 ... $\infty$ )	1.8 (1.2 ... 2.4)
CNRM-CM6-1 ssp585 (1)	$\infty$ (19 ... $\infty$ )	2.2 (1.3 ... 3.1)
CNRM-ESM2-1 ssp585 (1)	80 (3.1 ... $\infty$ )	2.1 (1.1 ... 3.1)
GFDL-CM4 ssp585 (1)	6.9e+7 (7.6 ... $\infty$ )	1.9 (0.90 ... 3.0)
HadGEM3-GC31-LL ssp585 (4)	21 (5.3 ... 1.2e+3)	2.1 (1.6 ... 2.6)
HadGEM3-GC31-MM ssp585 (4)	10.8 (3.7 ... 231)	2 (1.4 ... 2.6)

TaiESM1 ssp585 (1)	8.3 (1.9 ... ∞)	2.2 (0.9 ... 3.6)
HadGEM3-GA6-N216 (525)	60 (13.7 ... 3.4e+4)	2.3 (1.8 ... 3.0)

**Table 2.** Probability ratio and change in intensity of the 2022 event described by annual maximum of 2-day average daily mean temperature when compared with a 1.2°C cooler climate, from the models that passed the validation tests.

Model / Observations	Probability ratio PR [-]	Change in intensity $\Delta I$ [°C]
ERA5	5.0e+4 (9.7 ... ∞)	4.0 (2.6 ... 5.0)
CANESMr1-CCLM ()	8.0 (2.7 ... 1.0e+5)	2.1 (1.3 ... 2.9)
CANESMr1-REMO ()	3.6 (1.4 ... 1.5e+3)	0.96 (0.25 ... 1.6)
CNRMr1-CCLM ()	30 (2.3 ... 1.0e+5)	2.2 (1.1 ... 3.4)
CNRMr1-COSMOcrCLIM ()	1.0e+5 (6.9 ... 1.0e+5)	1.9 (0.24 ... 3.0)
CNRMr1-REMO ()	4.9e+5 (5.3 ... 1.0e+5)	2.9 (1.8 ... 4.3)
ECEARTHr12-COSMOcrCLIM ()	2.0 (0.88 ... 59)	0.70 (-0.16 ... 1.8)
ECEARTHr12-HIRHAM ()	2.1 (0.49 ... 1.0e+5)	0.49 (-0.42 ... 1.6)
ECEARTHr12-REMO ()	1.2 (0.36 ... 47)	0.18 (-0.98 ... 1.6)
ECEARTHr1-COSMOcrCLIM ()	3.4 (1.5 ... 1.0e+5)	1.4 (0.52 ... 2.3)
ECEARTHr1-HIRHAM ()	8.8 (1.8 ... 1.0e+5)	1.5 (0.69 ... 2.5)
ECEARTHr3-COSMOcrCLIM ()	1.4 (0.48 ... 9.6)	0.35 (-0.78 ... 1.5)
ECEARTHr3-HIRHAM ()	2.7 (0.53 ... 1.0e+5)	0.56 (-0.76 ... 1.6)
ECEARTHr3-RCA ()	1.9 (0.22 ... 1.0e+5)	0.32 (-0.93 ... 1.5)
MIROCr1-CCLM ()	2.1e+3 (6.5 ... 1.0e+5)	2.1 (1.1 ... 3.2)
MPIr1-COSMOcrCLIM ()	5.5 (1.8 ... 1.0e+5)	1.1 (0.13 ... 2.0)
MPIr1-HIRHAM ()	96 (5.1 ... 1.0e+5)	2.1 (0.99 ... 3.1)
MPIr1-RCA ()	1.0e+5 (2.4 ... 1.0e+5)	1.6 (0.27 ... 3.0)
MPIr2-COSMOcrCLIM ()	8.5 (0.84 ... 1.0e+5)	1.1 (-0.090 ... 2.1)
MPIr3-COSMOcrCLIM ()	2.1e+2 (2.6 ... 1.0e+5)	1.5 (0.14 ... 2.5)
NORESMr1-HADREM ()	7.6e+3 (3.8 ... 1.0e+5)	2.4 (0.98 ... 3.8)
NORESMr1-HIRHAM ()	13 (0.77 ... 1.0e+5)	1.1 (-0.23 ... 2.4)
NORESMr1-RACMO ()	10 (1.6 ... 1.0e+5)	1.4 (0.32 ... 2.6)
NORESMr1-RCA ()	86 (1.4 ... 1.0e+5)	1.5 (0.040 ... 3.1)
NORESMr1-REGCM ()	4.5 (1.7 ... 3.7e+7)	2.5 (1.1 ... 3.6)
NORESMr1-REMO ()	79 (1.2 ... 1.0e+5)	1.5 (0.16 ... 2.7)
NORESMr1-WRF381P ()	1.7 (0.88 ... 23)	1.0 (-0.18 ... 2.1)
ACCESS-CM2 ssp585 (4)	6.1 (3.1 ... 19)	1.6 (1.2 ... 2.1)
CNRM-CM6-1-HR ssp585 (1)	7.6 (1.9 ... ∞)	1.3 (0.39 ... 2.1)
EC-Earth3 ssp585 (5)	4.1 (2.6 ... 8.2)	1.2 (0.89 ... 1.6)
EC-Earth3-Veg-LR ssp585 (3)	3.3 (1.8 ... 8.5)	1.3 (0.71 ... 1.8)
GFDL-CM4 ssp585 (1)	23 (3.0 ... ∞)	1.6 (0.78 ... 2.4)
HadGEM3-GC31-MM ssp585 (4)	5.7 (3.2 ... 13.2)	1.7 (1.3 ... 2.1)
IPSL-CM6A-LR ssp585 (6)	59.5 (13.7 ... 2.6e+3)	1.7 (1.4 ... 2.0)
MIROC-ES2L ssp585 (10)	381 (62.3 ... 1.5e+4)	1.7 (1.5 ... 2.0)

MIROC6 ssp585 (50)	10.1 (7.5 ... 13.9)	1.3 (1.2 ... 1.5)
MRI-ESM2-0 ssp585 (6)	31.6 (10.5 ... 138)	1.5 (1.2 ... 1.9)
UKESM1-0-LL ssp585 (5)	4.1 (2.6 ... 7.9)	1.6 (1.2 ... 2)
HadGEM3-GA6-N216 (525)	12.1 (7.5 ... 148.8)	1.5 (1.3 ... 1.8)

## 6 Hazard synthesis

For the defined study area we calculate the probability ratio as well as the change in magnitude of the event in the observations and the models for both event definitions: 2022 maxima of 1-day maximum (Fig. 6) and 2-day average temperatures (Fig. 7). If the models do not pass the validation tests we do not use their results. We synthesise results from the models that pass validation (explained in Section 4) with the observational analysis to give an overarching attribution statement. Observations and models are combined into a single result in two ways. Firstly, we neglect common model uncertainties beyond the model spread that is depicted by the model average, and compute the weighted average of models and observations: this is indicated by the magenta bar. As, due to common model uncertainties, model uncertainty can be larger than the model spread, secondly, we also show the more conservative estimate of an unweighted average of observations and models, indicated by the white box around the magenta bar in the synthesis figures. For a detailed description of the synthesis procedure and statistical methods see [Li and Otto \(2022\)](#).

As has been observed in previous attribution studies on European heat waves (e.g. [Vautard et al., 2019](#)), climate models show a systematically lower trend than the observations which in particular means that the change in intensity in the models is much lower than in observations. They also often show too high variability. Even for models that do capture the trend, this often happens for the wrong reasons as has been assessed in van Oldenborgh et al. ([2022](#)). Using De Bilt in the Netherlands as an example they found that in many locations the discrepancies between observed and modelled trends are much larger than can be expected on the basis of natural variability and model spread alone. Because of this systematic discrepancy, providing quantitative synthesised estimates of the change in intensity and frequency is difficult as the upper bound is very ill defined and largely infinite, while the lower bound is almost certainly an underestimation given the model deficiencies.

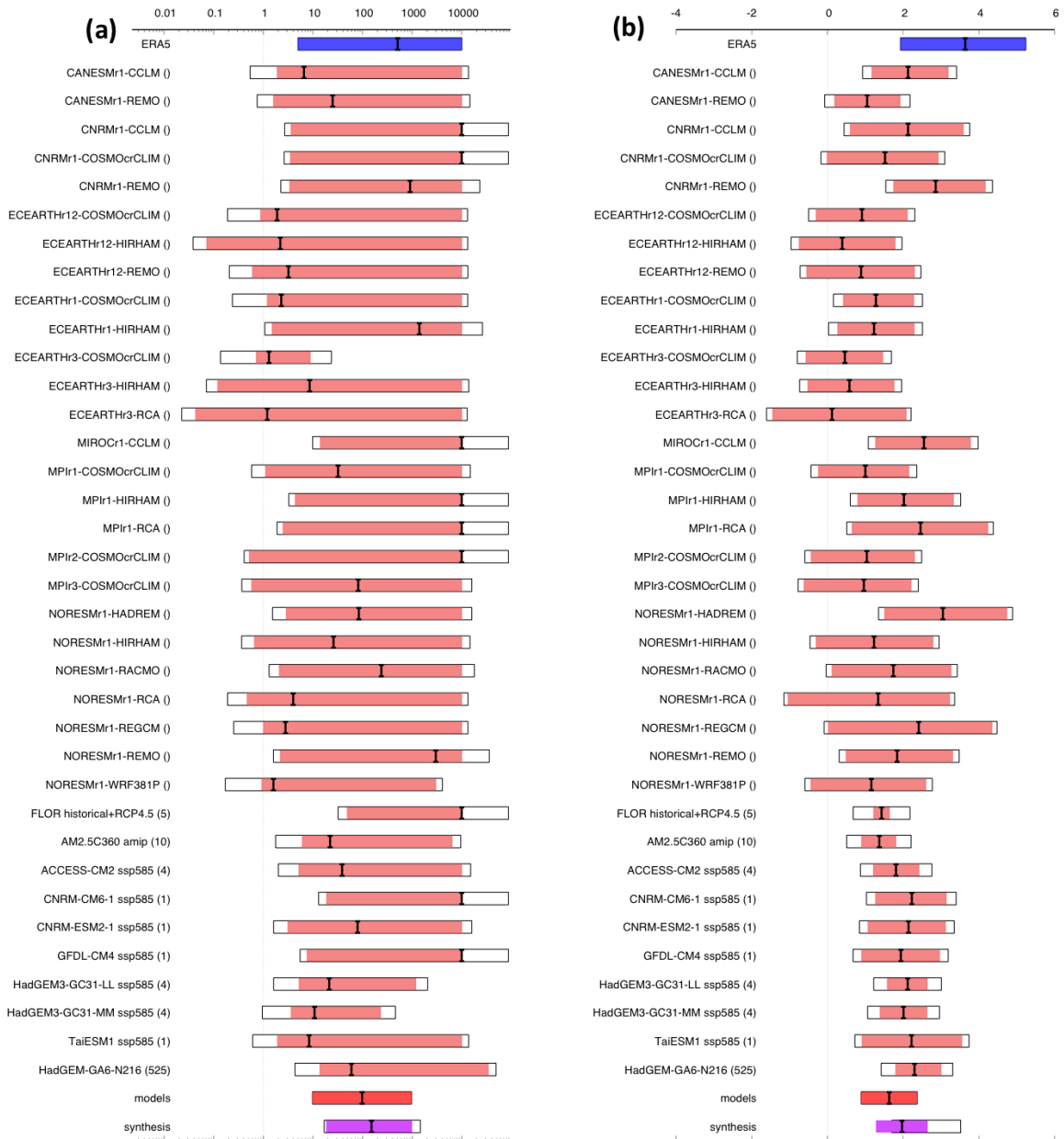


Fig. 6 Synthesis of (a) probability ratios and (b) intensity changes when comparing the return period and magnitudes of the 2022 maximum of 1-day maximum daily temperature event in the current climate and a 1.2°C cooler climate.

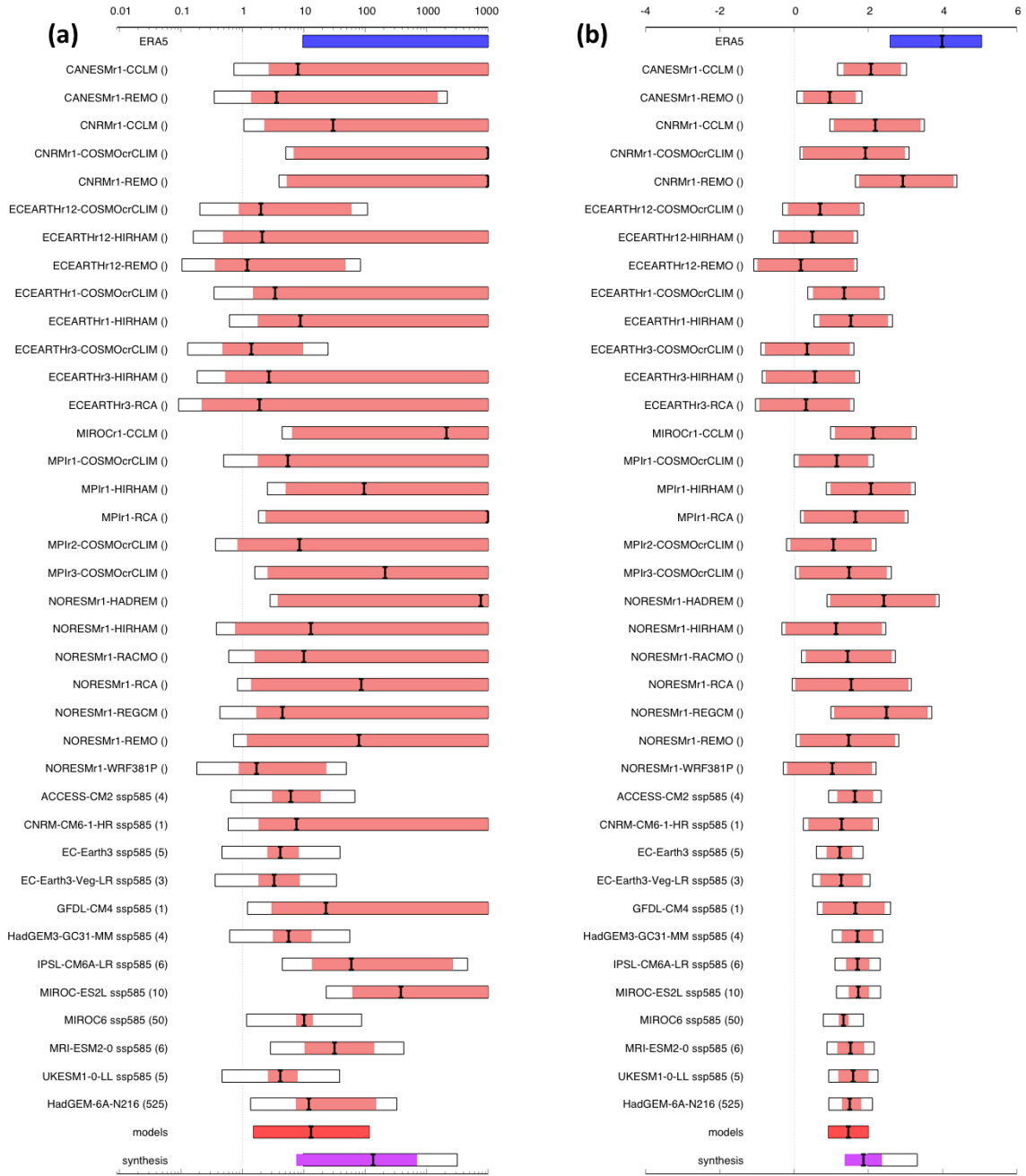


Fig. 7 Synthesis of (a) probability ratios and (b) intensity changes when comparing the return period and magnitudes of the 2022 maximum of 2-day mean daily temperature event in the current climate and a 1.2°C cooler climate.

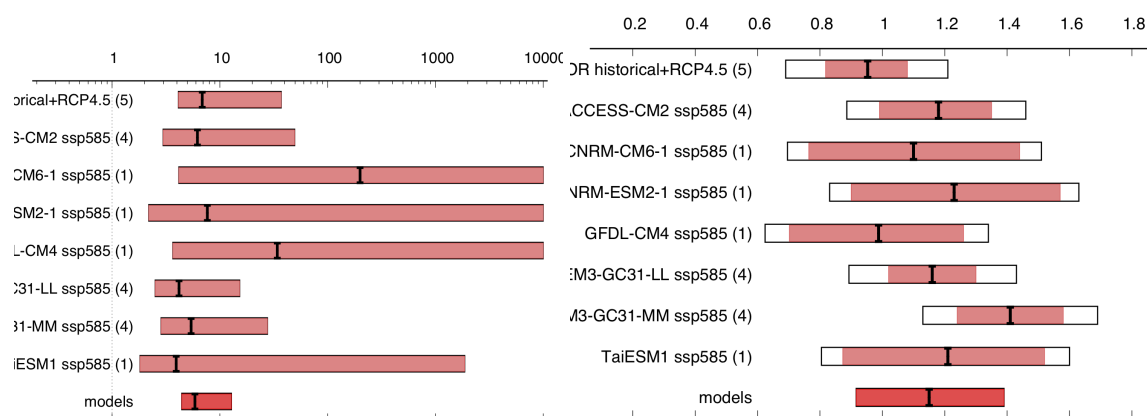


Fig. 8 As figure S, but for models only of a 0.8°C warmer (2°C since pre-industrial) climate.

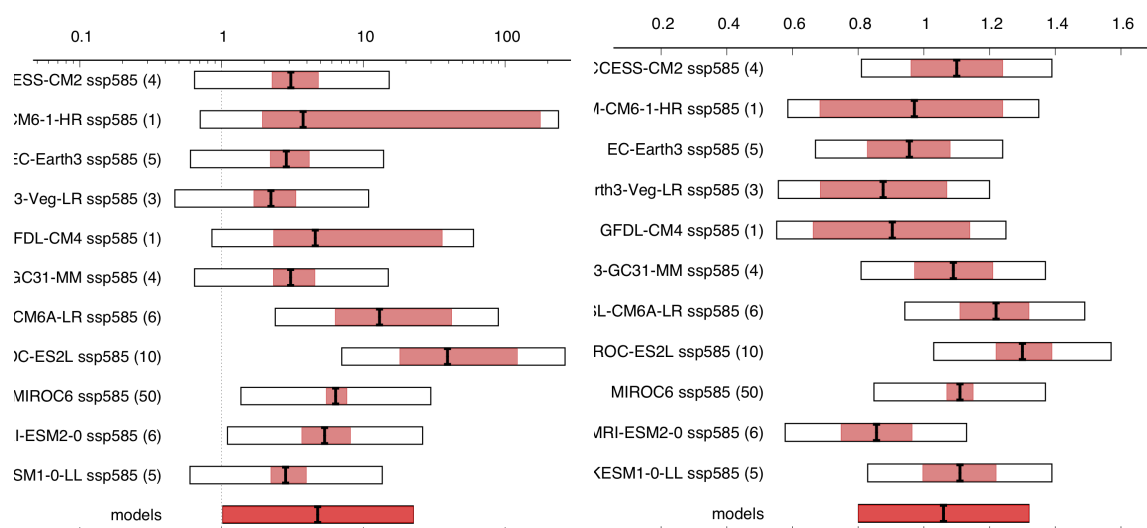


Fig. 9 As figure T, but for models only of a 0.8°C warmer (2°C since pre-industrial) climate.

Figures 6 and 7 show an overview of the synthesised results for both event definitions. For the change in frequency the lower bound of the change due to human-induced climate change is a rounded 10 times increase (9 for TXx, 17 for 2-day Tmean). The change in intensity is only about 2°C in the models, while it is 4°C in the observations. We thus do not report a combined estimate but both figures separately.

Figures 8 and 9 show the same as Figures 6 and 7 but for changes in frequency and intensity of such a heatwave to occur in a 0.8°C warmer world compared to today. For both event definitions a further increase in intensity of about 1°C is shown as well as an up to 10 times further increase in the frequency of such an event. Given the discrepancies between models and observations the confidence in these numbers is however low, and they are very likely an underestimation of future changes.

## 7 Vulnerability and exposure

Risk should be conceptualised “as the potential for adverse consequences” (Reisinger et al, 2020) and includes interplay between a hazard (here the heatwave), and the exposure, vulnerability, and coping capacity of people, infrastructure, and systems who experience it (IPCC SREX, 2019). Many factors contributed to the impacts caused by this particular heatwave, a combination of the unprecedented

high temperatures experienced, preparedness, early warning, and response systems, infrastructure and urban planning, and differential vulnerabilities of certain demographics. Active adaptation on all fronts, resilience-building, and mitigation measures can significantly help to reduce the impacts of events such as this ([Raju, Boyd, and Otto, 2022](#)).

First, the United Kingdom has very little experience with extreme high temperatures - a reality which has highlighted heat as an “invisible risk” of both policy and research in the country ([Brimicombe et al, 2021](#)). Along with much of Europe, the United Kingdom was severely impacted during the record breaking heatwaves in 2003. In 2018 and 2019, the country also experienced record breaking heat waves but of these of lower temperatures than the recent one (MacCarthy et al. 2019; [Met Office, 2019](#)). The July 2022 heatwave broke new records, with over 40 degrees Celsius recorded in different parts of the country, including London. It was the first time those temperatures had ever been recorded, beating previous records by at least 1 or 2 degrees Celsius. ([Met Office, 2022a](#)). It is well-understood that experience with hydrometeorological extremes is key to resilience of systems, infrastructure, and individuals and a key driver motivating and/or shaping climate adaptation ([van Valkengoed and Steg, 2019](#); [Demski et al. 2017](#)). In this way, the United Kingdom’s limited experience with extreme high temperatures makes the country particularly exposed and vulnerable to devastating heat impacts with unadapted infrastructure, limited systems and knowledge about behaviours to adopt during extreme heat ([Brimicombe et al, 2021](#))

Second, the United Kingdom has certain policies and systems meant to prepare the country for extreme heat in different ways. First published in 2004, following the 2003 heatwave impacts, but significantly updated in 2012, the “Heatwave Plan for England” is the government’s comprehensive heat action plan that lays out the actions from long-term risk reduction to seasonal preparedness to early warning to heatwave actions and declaration of a national emergency ([Heatwave Plan, 2012](#)).

This particular heatwave was well captured by models and forecasts, and provided time for authorities to act before the peak of the heat. On the 16th of July, the UK Met Office emitted the country’s first ever “amber” extreme heat alert, defined as a national emergency (and complementing the raising of warning levels by the country’s Health Security Agency) for when a heatwave is: “*so severe and/or prolonged that its effects extend outside the health and social care system. At this level, illness and death may occur among the fit and healthy, and not just in high-risk groups*” ([UK Met Office 2022b](#)). Temperatures and mortality as well as hospitalisations have been shown to be positively correlated in England, and strains on health services was certainly seen during this event with notably the National Health Service calling on the government for additional resources ([BMJ, 2022](#)). The warnings were relatively widely communicated to institutions and the public through local authorities and the media throughout the heatwave period. However, early warning does not always translate into early action, and in-depth reviews will be required to understand the effectiveness of the system for this event. An evaluation of the Heatwave Plan was conducted in 2019 showed mixed results about the effectiveness of the plan in reducing mortality and hospitalisations, and offered a range of recommendations to increase the reach of messages, institutional support, and more ([PIRU, 2019](#)). For the July 2022 heatwave, preliminary analysis, using peer-reviewed methodology ([Gasparinni et al. 2022](#)) projects excess mortality of over 840 people in England and Wales on July 18 and 19 with mortality highest for people ages 85 and over ([Gasparrini, 19 July, 2022](#)). Official excess mortality figures will be available in the coming months however, a standard frame of time for heat-related mortality calculations.

Third, during the heatwave, much was discussed about the UK housing’s limited ability to withstand heat. Traditionally, British infrastructure that was built to retain heat and air conditioning is rare. In 2021, the UK Climate Change Committee warned that over 570,000 homes were not resilient to high temperatures, making many of them uninhabitable ([CCC, 2022](#)). This was certainly visible in the noted impacts of the July heatwave with people seeking shelter from their sweltering homes on the street, in parks, on beaches. In London, this reality was compounded for many residents by the urban heat island effect making the city significantly warmer than surrounding areas ([Mayor of London, u.d.](#); [Goddard and Tett, 2019](#); [Chowienczyk et al. 2020](#)) Even within London itself, there are high

levels of inequity in experienced temperatures, with certain, often poorer neighbourhoods, lacking green space, shade, and water which can be lifelines during heatwave. Previous research has shown that London has a particularly inequitable Urban Heat Island effect ([Chakraborty et al. 2019](#)).

Finally, as recently seen in other parts of the world such as South Asia ([Zachariah et al. 2022](#)), heatwave impacts are also unequally distributed across demographics due to a range of physiological, psychological and socio-economic factors. For instance, older people and people with chronic health conditions are at heightened risk of dying during heatwaves (Oudin [Aström et al. 2015](#)). The highest risk of dying has also been associated with being confined to a bed, not being able to leave the home regularly, and with limited self-care abilities ([Bouchama et al. 2017](#)). Heatwaves have the potential to not only impact physical health but also mental health and wellbeing (Kelman, 2022). Certain studies have shown the strength of social networks can significantly decrease some of these vulnerabilities ([Klinenberg, 2015](#); [Bouchama et al. 2017](#)). Children also present particular physical vulnerabilities to extreme heat ([Xu et al. 2014](#)). Other groups have been shown to have particular vulnerability and exposure characteristics which shape their experience with extreme heat. For instance, homeless people ([Schwarz et al. 2021](#)) and incarcerated people are particularly exposed and often have limited support to cope ([Colluci et al. 2021](#)). Finally, existing health inequalities, notably in the UK for Black Asian and Ethnic Minority (BAME) ([Keys et al. 2021](#)), brought to light particularly by the COVID-19 pandemic will have echoes on health impacts during heatwaves ([Parks and Thalheimer, 2020](#)). All these differential vulnerabilities were observed across the UK and in London during this event, and showcase how the same extreme weather impacts different people in different ways, with different magnitudes, requiring different adaptation measures.

### **Data availability**

*Almost all data are or will soon be available via the Climate Explorer.  
For access to weather station data please contact the UK Met Office.*

## Supplementary Material

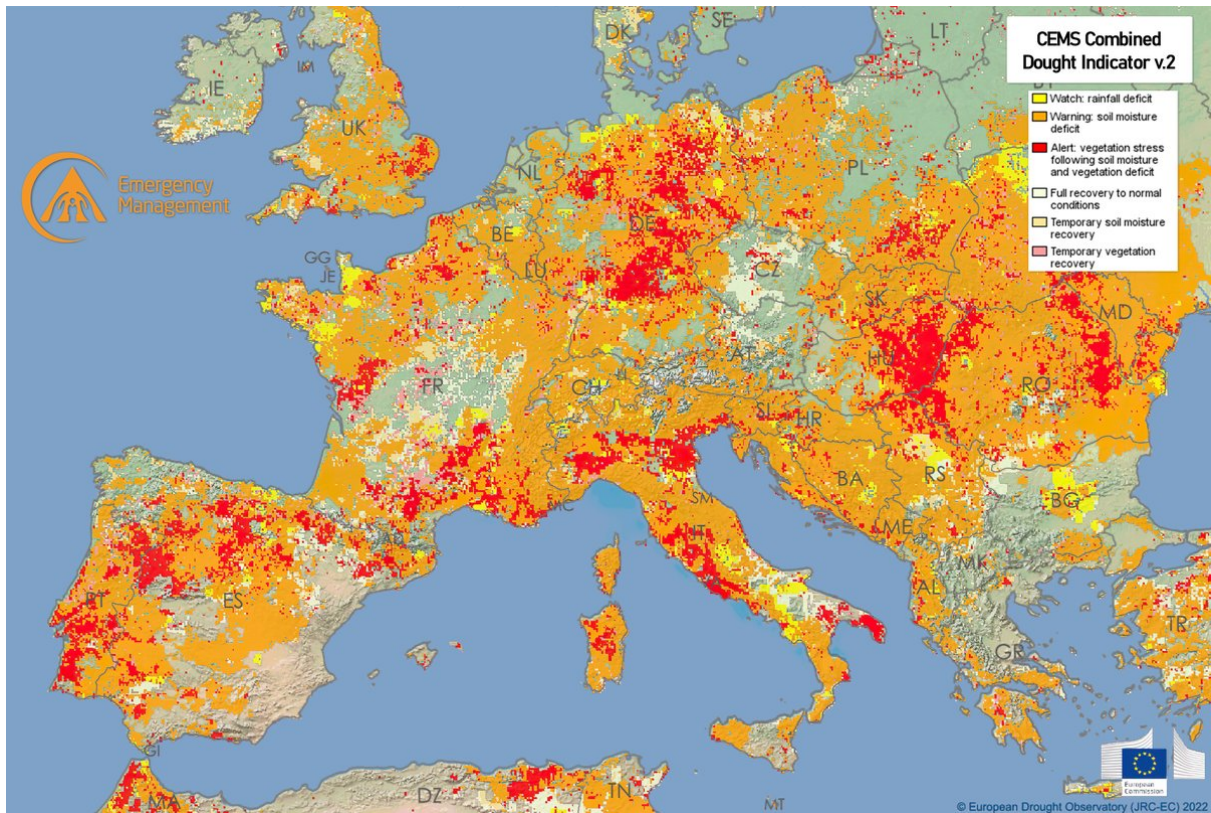


**Figure S1:** Observed drought conditions across Europe, for the ten days from July 01-10 2022. Orange and red areas indicate drought ‘warning’ and ‘alert’ conditions, respectively. Source: European Drought Observatory (<https://edo.jrc.ec.europa.eu/edov2/php/index.php?id=1000>).

**Table S1.** Evaluation results for the climate models considered for the attribution analysis of the 2022 daily maximum temperature, for the study region. The table contains estimates for dispersion parameter, and event magnitude. The corresponding estimates from the ERA5 dataset is shown in blue. The models that are selected for attributing this event are highlighted in green.

Observed data	Scale parameter	Shape parameter
ERA5 (1950-2022)	1.68 (1.36 ... 1.95)	-0.11 (-0.31 ... 0.045)
Model	Scale parameter	Shape parameter
CANESMr1-CCLM ()	1.77 (1.37 ... 2.06)	-0.060 (-0.24 ... 0.13)
CANESMr1-REMO ()	1.66 (1.26 ... 1.97)	-0.19 (-0.33 ... -0.030)
CNRMr1-ALADIN53 ()	1.99 (1.46 ... 2.40)	-0.10 (-0.42 ... 0.18)
CNRMr1-ALADIN63 ()	2.34 (1.92 ... 2.71)	-0.20 (-0.36 ... -0.070)
CNRMr1-CCLM ()	1.66 (1.37 ... 1.89)	-0.20 (-0.51 ... -0.070)
CNRMr1-COSMOcrCLIM ()	1.65 (1.24 ... 1.96)	-0.24 (-0.42 ... -0.040)
CNRMr1-HADREM ()	2.27 (1.75 ... 2.67)	-0.13 (-0.32 ... 0.040)
CNRMr1-HIRHAM ()	1.81 (1.46 ... 2.14)	-0.32 (-0.58 ... -0.17)

CNRMr1-RACMO ()	2.02 (1.68 ... 2.31)	-0.19 (-0.37 ... -0.040)
CNRMr1-RCA ()	1.91 (1.49 ... 2.28)	-0.37 (-0.74 ... -0.17)
CNRMr1-REGCM ()	2.09 (1.64 ... 2.50)	-0.14 (-0.56 ... 0.11)
CNRMr1-REMO ()	1.48 (1.15 ... 1.74)	-0.12 (-0.49 ... 0.12)
CNRMr1-WRF381P ()	2.58 (2.09 ... 3.09)	-0.51 (-0.81 ... -0.30)
ECEARTHr12-CCLM ()	1.94 (1.57 ... 2.33)	-0.050 (-0.32 ... 0.13)
ECEARTHr12-COSMOcrCLIM ()	1.56 (1.28 ... 1.83)	-0.020 (-0.22 ... 0.16)
ECEARTHr12-HADREM ()	1.98 (1.59 ... 2.41)	-0.070 (-0.42 ... 0.070)
ECEARTHr12-HIRHAM ()	1.51 (1.06 ... 1.79)	-0.16 (-0.36 ... 0.090)
ECEARTHr12-RACMO ()	2.06 (1.71 ... 2.39)	-0.17 (-0.51 ... -0.040)
ECEARTHr12-RCA ()	2.50 (1.95 ... 3.05)	-0.17 (-0.42 ... 0.020)
ECEARTHr12-REGCM ()	2.95 (2.36 ... 3.49)	-0.14 (-0.55 ... 0.090)
ECEARTHr12-REMO ()	1.54 (1.14 ... 1.86)	-0.090 (-0.26 ... 0.14)
ECEARTHr12-WRF361H ()	2.32 (1.68 ... 2.80)	-0.010 (-0.16 ... 0.19)
ECEARTHr12-WRF381P ()	2.62 (2.12 ... 3.07)	-0.16 (-0.41 ... 0.040)
ECEARTHr1-COSMOcrCLIM ()	1.67 (1.22 ... 1.98)	-0.010 (-0.18 ... 0.25)
ECEARTHr1-HIRHAM ()	1.41 (1.16 ... 1.62)	-0.21 (-0.44 ... -0.080)
ECEARTHr1-RACMO ()	2.10 (1.69 ... 2.45)	-0.18 (-0.43 ... -0.040)
ECEARTHr1-RCA ()	2.21 (1.58 ... 2.68)	-0.070 (-0.32 ... 0.14)
ECEARTHr3-COSMOcrCLIM ()	1.47 (1.18 ... 1.70)	0.030 (-0.16 ... 0.21)
ECEARTHr3-HIRHAM ()	1.56 (1.28 ... 1.88)	-0.22 (-0.61 ... -0.10)
ECEARTHr3-RCA ()	1.75 (1.26 ... 2.12)	-0.14 (-0.48 ... 0.15)
ECEARTHr3-RACMO ()	2.10 (1.72 ... 2.38)	-0.29 (-0.50 ... -0.16)
HADGEMr1-ALADIN63 ()	2.46 (2.00 ... 2.89)	-0.34 (-0.64 ... -0.21)
HADGEMr1-CCLM ()	2.06 (1.71 ... 2.40)	-0.29 (-0.52 ... -0.12)
HADGEMr1-COSMOcrCLIM ()	2.11 (1.61 ... 2.44)	-0.12 (-0.34 ... 0.030)
HADGEMr1-HADREM ()	2.11 (1.69 ... 2.45)	-0.21 (-0.41 ... -0.050)
HADGEMr1-HIRHAM ()	1.66 (1.35 ... 1.99)	-0.16 (-0.49 ... 0.020)
HADGEMr1-RACMO ()	2.36 (1.79 ... 2.80)	-0.40 (-0.76 ... -0.17)
HADGEMr1-RCA ()	2.43 (1.75 ... 3.05)	-0.15 (-0.46 ... 0.16)
HADGEMr1-REGCM ()	1.88 (1.43 ... 2.30)	0.040 (-0.20 ... 0.27)
HADGEMr1-REMO ()	1.87 (1.38 ... 2.28)	-0.25 (-0.62 ... -0.12)
HADGEMr1-WRF361H ()	2.90 (2.16 ... 3.48)	-0.28 (-0.58 ... -0.040)
HADGEMr1-WRF381P ()	2.50 (2.04 ... 2.91)	-0.39 (-0.60 ... -0.24)
IPSLr1-HIRHAM ()	2.35 (1.88 ... 2.80)	-0.37 (-0.60 ... -0.17)
IPSLr1-RACMO ()	2.76 (2.21 ... 3.25)	-0.18 (-0.36 ... 0.0)
IPSLr1-REMO ()	2.03 (1.63 ... 2.33)	-0.24 (-0.52 ... 0.030)
IPSLr1-RCA ()	2.48 (1.85 ... 2.98)	-0.16 (-0.49 ... 0.0)
IPSLr1-WRF381P ()	2.45 (1.95 ... 3.15)	-0.58 (-1.1 ... -0.40)
MIROCr1-CCLM ()	1.71 (1.41 ... 1.97)	-0.27 (-0.51 ... -0.10)

MIROCr1-REMO ()	1.34 (1.12 ... 1.53)	-0.12 (-0.32 ... 0.040)
MPi1r1-ALADIN63 ()	3.00 (2.32 ... 3.54)	-0.20 (-0.40 ... 0.0)
MPi1r1-CCLM ()	2.14 (1.52 ... 2.70)	-0.39 (-0.76 ... 0.060)
MPi1r1-COSMOcrCLIM ()	1.70 (1.41 ... 1.94)	-0.21 (-0.53 ... -0.030)
MPi1r1-HADREM ()	2.20 (1.75 ... 2.54)	-0.21 (-0.40 ... -0.060)
MPi1r1-HIRHAM ()	1.82 (1.48 ... 2.13)	-0.21 (-0.48 ... -0.050)
MPi1r1-RACMO ()	2.24 (1.78 ... 2.65)	-0.22 (-0.54 ... 0.010)
MPi1r1-RCA ()	1.86 (1.45 ... 2.19)	-0.24 (-0.49 ... -0.030)
MPi1r1-REGCM ()	2.91 (2.12 ... 3.47)	-0.25 (-0.49 ... 0.010)
MPi1r1-REMO ()	1.67 (1.30 ... 1.93)	-0.12 (-0.39 ... 0.070)
MPi1r1-WRF361H ()	2.94 (2.26 ... 3.85)	-0.48 (-1.1 ... -0.31)
MPi1r1-WRF381P ()	2.67 (2.12 ... 3.13)	-0.26 (-0.44 ... -0.11)
MPi2r2-COSMOcrCLIM ()	1.72 (1.40 ... 2.00)	-0.26 (-0.53 ... -0.11)
MPi2r2-RCA ()	1.98 (1.54 ... 2.29)	-0.28 (-0.47 ... -0.090)
MPi2r2-REMO ()	2.15 (1.71 ... 2.51)	-0.33 (-0.53 ... -0.20)
MPi3r3-COSMOcrCLIM ()	1.71 (1.36 ... 2.01)	-0.23 (-0.56 ... -0.060)
MPi3r3-RCA ()	2.16 (1.68 ... 2.66)	-0.14 (-0.51 ... 0.080)
MPi3r3-REMO ()	2.08 (1.65 ... 2.41)	-0.33 (-0.61 ... -0.22)
NOESMr1-ALADIN63 ()	2.01 (1.59 ... 2.32)	-0.15 (-0.33 ... 0.010)
NOESMr1-COSMOcrCLIM ()	1.31 (0.990 ... 1.58)	-0.090 (-0.32 ... 0.15)
NOESMr1-HADREM ()	1.72 (1.36 ... 2.05)	-0.10 (-0.26 ... 0.060)
NOESMr1-HIRHAM ()	1.61 (1.35 ... 1.85)	-0.17 (-0.34 ... -0.010)
NOESMr1-RACMO ()	1.87 (1.50 ... 2.17)	-0.19 (-0.38 ... -0.020)
NOESMr1-RCA ()	1.79 (1.32 ... 2.15)	-0.080 (-0.32 ... 0.18)
NOESMr1-REGCM ()	1.92 (1.45 ... 2.31)	0.030 (-0.22 ... 0.30)
NOESMr1-REMO ()	1.45 (1.19 ... 1.74)	-0.18 (-0.36 ... -0.020)
NOESMr1-WRF381P ()	1.80 (1.43 ... 2.15)	0.040 (-0.32 ... 0.26)
FLOR historical+RCP4.5 (5)	2.27 (2.09 ... 2.42)	-0.29 (-0.35 ... -0.22)
AM2.5C360 amip (10)	2.19 (2.07 ... 2.32)	-0.18 (-0.23 ... -0.14)
ACCESS-CM2 ssp585 (4)	1.51 (1.01 ... 2.02)	-0.18 (-0.22 ... -0.13)
ACCESS-ESM1-5 ssp585 (40)	1.87 (1.66 ... 2.08)	-0.20 (-0.21 ... -0.18)
AWI-CM-1-1-MR ssp585 (1)	1.10 (0.549 ... 1.67)	-0.30 (-0.39 ... -0.21)
CAMS-CSM1-0 ssp585 (1)	1.07 (-0.0910 ... 2.24)	-0.11 (-0.18 ... -0.027)
CMCC-CM2-SR5 ssp585 (1)	1.57 (0.889 ... 2.21)	-0.070 (-0.17 ... 0.044)
CMCC-ESM2 ssp585 (1)	1.40 (0.400 ... 2.37)	-0.11 (-0.18 ... -0.0080)
CNRM-CM6-1 ssp585 (1)	1.86 (1.06 ... 2.62)	-0.24 (-0.31 ... -0.16)
CNRM-CM6-1-HR ssp585 (1)	1.14 (0.278 ... 2.01)	-0.26 (-0.37 ... -0.15)
CNRM-ESM2-1 ssp585 (1)	1.78 (0.889 ... 2.60)	-0.15 (-0.26 ... -0.037)
CanESM5 ssp585 (50)	1.03 (0.973 ... 1.09)	-0.20 (-0.21 ... -0.19)
EC-Earth3 ssp585 (5)	0.428 (0.0490 ... 0.795)	-0.20 (-0.23 ... -0.16)

EC-Earth3-Veg ssp585 (7)	0.147 (-0.186 ... 0.483)	-0.17 (-0.20 ... -0.14)
EC-Earth3-Veg-LR ssp585 (3)	0.619 (-0.0240 ... 1.26)	-0.20 (-0.25 ... -0.14)
FGOALS-g3 ssp585 (3)	0.711 (0.243 ... 1.18)	-0.26 (-0.30 ... -0.20)
GFDL-CM4 ssp585 (1)	1.62 (0.752 ... 2.47)	-0.20 (-0.27 ... -0.12)
GFDL-ESM4 ssp585 (1)	0.320 (-0.829 ... 1.47)	-0.22 (-0.32 ... -0.11)
HadGEM3-GC31-LL ssp585 (4)	1.77 (1.32 ... 2.20)	-0.13 (-0.17 ... -0.084)
HadGEM3-GC31-MM ssp585 (4)	1.67 (1.16 ... 2.19)	-0.12 (-0.16 ... -0.073)
INM-CM4-8 ssp585 (1)	2.03 (0.482 ... 3.64)	-0.22 (-0.30 ... -0.11)
INM-CM5-0 ssp585 (1)	3.17 (1.33 ... 4.88)	-0.24 (-0.32 ... -0.15)
IPSL-CM6A-LR ssp585 (6)	1.27 (0.953 ... 1.59)	-0.27 (-0.30 ... -0.23)
MIROC-ES2L ssp585 (10)	1.20 (0.954 ... 1.47)	-0.22 (-0.24 ... -0.20)
MIROC6 ssp585 (50)	1.01 (0.866 ... 1.15)	-0.17 (-0.18 ... -0.16)
MPI-ESM1-2-HR ssp585 (2)	0.611 (0.110 ... 1.10)	-0.24 (-0.29 ... -0.17)
MPI-ESM1-2-LR ssp585 (30)	0.131 (-0.021 ... 0.277)	-0.23 (-0.24 ... -0.23)
MRI-ESM2-0 ssp585 (6)	1.16 (0.839 ... 1.46)	-0.23 (-0.26 ... -0.20)
NorESM2-MM ssp585 (1)	2.90 (1.46 ... 4.36)	-0.28 (-0.37 ... -0.18)
TaiESM1 ssp585 (1)	1.85 (0.760 ... 2.96)	-0.085 (-0.17 ... 0.020)
UKESM1-0-LL ssp585 (5)	1.19 (0.674 ... 1.69)	-0.17 (-0.21 ... -0.12)
CNRM-CM6-1-HR highresmpip	2.385 (1.965... 2.791)	-0.204 (-0.414... -0.069)
EC-Earth3P-HR highresmpip	1.967 (1.583... 2.298)	-0.225 (-0.427... -0.044)
MRI-AGCM3-2-H highresmpip	2.575 (1.979... 2.993)	-0.012 (-0.194... 0.147)
MRI-AGCM3-2-S highresmpip	2.355 (1.872... 2.832)	-0.099 (-0.375... .131)
HadGEM3-GA6-N216 (525)	0.704 (0.57 ... 0.796)	-0.227 (-0.476...-0.071)

**Table S2.** Evaluation results for the climate models considered for the attribution analysis of the 2022 maximum 2-day average mean temperature, for the study region. The table contains estimates for dispersion parameter, and event magnitude. The corresponding estimates from the ERA5 dataset is shown in blue. The models that are selected for attributing this event are highlighted in green.

Observed data	Scale parameter	Shape parameter
ERA5 (1950-2022)	1.28 (0.955 ... 1.53)	-0.13 (-0.28 ... 0.11)
Model	Scale parameter	Shape parameter
CANESMr1-CCLM ()	1.46 (1.19 ... 1.67)	-0.070 (-0.29 ... 0.070)
CANESMr1-REMO ()	1.31 (1.03 ... 1.53)	-0.11 (-0.24 ... 0.060)
CNRMr1-ALADIN53 ()	1.50 (1.11 ... 1.81)	-0.22 (-0.40 ... 0.050)
CNRMr1-ALADIN63 ()	1.62 (1.27 ... 1.88)	-0.19 (-0.34 ... -0.020)
CNRMr1-CCLM ()	1.33 (1.01 ... 1.55)	-0.12 (-0.50 ... 0.090)
CNRMr1-COSMOcrCLIM ()	1.34 (1.02 ... 1.63)	-0.24 (-0.57 ... -0.010)
CNRMr1-HADREM ()	1.68 (1.31 ... 1.97)	-0.13 (-0.32 ... 0.010)

CNRMr1-HIRHAM ()	1.62 (1.28 ... 1.93)	-0.25 (-0.40 ... -0.090)
CNRMr1-RACMO ()	1.43 (1.17 ... 1.65)	-0.16 (-0.33 ... 0.0)
CNRMr1-RCA ()	1.29 (0.960 ... 1.53)	-0.23 (-0.48 ... 0.030)
CNRMr1-REGCM ()	1.44 (1.15 ... 1.70)	-0.070 (-0.33 ... 0.10)
CNRMr1-REMO ()	1.45 (1.14 ... 1.68)	-0.19 (-0.43 ... 0.040)
CNRMr1-WRF381P ()	2.10 (1.73 ... 2.41)	-0.39 (-0.58 ... -0.23)
ECEARTHr12-CCLM ()	1.58 (1.20 ... 2.01)	-0.070 (-0.40 ... 0.14)
ECEARTHr12-COSMOcrCLIM ()	1.19 (0.970 ... 1.39)	-0.030 (-0.21 ... 0.13)
ECEARTHr12-HADREM ()	1.54 (1.23 ... 1.82)	-0.12 (-0.39 ... 0.030)
ECEARTHr12-HIRHAM ()	1.22 (0.840 ... 1.44)	-0.12 (-0.33 ... 0.16)
ECEARTHr12-RACMO ()	1.47 (1.17 ... 1.73)	-0.18 (-0.42 ... 0.020)
ECEARTHr12-RCA ()	1.46 (1.09 ... 1.84)	0.0 (-0.33 ... 0.20)
ECEARTHr12-REGCM ()	2.18 (1.65 ... 2.65)	-0.13 (-0.48 ... 0.12)
ECEARTHr12-REMO ()	1.37 (1.09 ... 1.64)	-0.060 (-0.23 ... 0.12)
ECEARTHr12-WRF361H ()	1.40 (1.08 ... 1.70)	0.15 (-0.030 ... 0.37)
ECEARTHr12-WRF381P ()	1.96 (1.57 ... 2.30)	-0.11 (-0.33 ... 0.090)
ECEARTHr1-COSMOcrCLIM ()	1.39 (1.09 ... 1.62)	-0.040 (-0.24 ... 0.12)
ECEARTHr1-HIRHAM ()	1.18 (0.970 ... 1.40)	-0.090 (-0.36 ... 0.10)
ECEARTHr1-RACMO ()	1.44 (1.16 ... 1.71)	-0.060 (-0.26 ... 0.11)
ECEARTHr1-RCA ()	1.41 (1.00 ... 1.69)	-0.040 (-0.29 ... 0.29)
ECEARTHr3-COSMOcrCLIM ()	1.32 (0.990 ... 1.55)	-0.070 (-0.20 ... 0.17)
ECEARTHr3-HIRHAM ()	1.42 (1.14 ... 1.65)	-0.18 (-0.51 ... -0.060)
ECEARTHr3-RCA ()	1.08 (0.800 ... 1.29)	-0.15 (-0.46 ... 0.090)
ECEARTHr3-RACMO ()	1.50 (1.21 ... 1.77)	-0.33 (-0.55 ... -0.14)
HADGEMr1-ALADIN63 ()	1.89 (1.48 ... 2.19)	-0.22 (-0.47 ... -0.040)
HADGEMr1-CCLM ()	1.60 (1.31 ... 1.86)	-0.23 (-0.40 ... -0.060)
HADGEMr1-COSMOcrCLIM ()	1.60 (1.17 ... 1.85)	-0.13 (-0.39 ... 0.070)
HADGEMr1-HADREM ()	1.52 (1.21 ... 1.79)	-0.18 (-0.35 ... -0.010)
HADGEMr1-HIRHAM ()	1.67 (1.26 ... 1.99)	-0.23 (-0.46 ... -0.030)
HADGEMr1-RACMO ()	1.79 (1.39 ... 2.10)	-0.37 (-0.65 ... -0.20)
HADGEMr1-RCA ()	1.59 (1.18 ... 1.97)	-0.080 (-0.31 ... 0.17)
HADGEMr1-REGCM ()	1.37 (0.990 ... 1.77)	0.15 (-0.12 ... 0.44)
HADGEMr1-REMO ()	1.76 (1.33 ... 2.11)	-0.28 (-0.59 ... -0.14)
HADGEMr1-WRF361H ()	1.74 (1.20 ... 2.12)	-0.030 (-0.25 ... 0.32)
HADGEMr1-WRF381P ()	2.00 (1.63 ... 2.34)	-0.41 (-0.64 ... -0.27)
IPSLr1-HIRHAM ()	1.80 (1.44 ... 2.13)	-0.18 (-0.38 ... 0.010)
IPSLr1-RACMO ()	1.86 (1.54 ... 2.16)	-0.14 (-0.29 ... -0.040)
IPSLr1-REMO ()	1.79 (1.45 ... 2.10)	-0.25 (-0.47 ... -0.040)

IPSLr1-RCA ()	1.56 (1.13 ... 1.93)	-0.10 (-0.38 ... 0.16)
IPSLr1-WRF381P ()	2.04 (1.66 ... 2.47)	-0.46 (-0.83 ... -0.29)
MIROCr1-CCLM ()	1.33 (1.09 ... 1.52)	-0.20 (-0.40 ... -0.040)
MIROCr1-REMO ()	1.30 (1.07 ... 1.50)	-0.17 (-0.38 ... 0.010)
MPIr1-ALADIN63 ()	2.29 (1.81 ... 2.67)	-0.20 (-0.39 ... -0.040)
MPIr1-CCLM ()	1.71 (1.31 ... 2.07)	-0.25 (-0.52 ... 0.040)
MPIr1-COSMOcrCLIM ()	1.23 (0.970 ... 1.45)	-0.11 (-0.34 ... 0.070)
MPIr1-HADREM ()	1.71 (1.33 ... 2.01)	-0.27 (-0.48 ... -0.13)
MPIr1-HIRHAM ()	1.51 (1.23 ... 1.73)	-0.18 (-0.40 ... 0.010)
MPIr1-RACMO ()	1.70 (1.30 ... 2.02)	-0.15 (-0.36 ... 0.060)
MPIr1-RCA ()	1.31 (0.970 ... 1.57)	-0.26 (-0.53 ... -0.10)
MPIr1-REGCM ()	2.08 (1.49 ... 2.50)	-0.11 (-0.30 ... 0.20)
MPIr1-REMO ()	1.60 (1.22 ... 1.85)	-0.14 (-0.40 ... 0.010)
MPIr1-WRF361H ()	1.95 (1.54 ... 2.32)	-0.27 (-0.64 ... -0.060)
MPIr1-WRF381P ()	1.99 (1.56 ... 2.30)	-0.17 (-0.37 ... 0.070)
MPIr2-COSMOcrCLIM ()	1.34 (1.04 ... 1.57)	-0.18 (-0.36 ... -0.030)
MPIr2-RCA ()	1.48 (1.16 ... 1.78)	-0.28 (-0.56 ... -0.090)
MPIr2-REMO ()	2.02 (1.66 ... 2.36)	-0.31 (-0.57 ... -0.20)
MPIr3-COSMOcrCLIM ()	1.43 (1.21 ... 1.64)	-0.23 (-0.51 ... -0.12)
MPIr3-RCA ()	1.32 (0.970 ... 1.68)	0.010 (-0.28 ... 0.34)
MPIr3-REMO ()	1.90 (1.49 ... 2.24)	-0.32 (-0.50 ... -0.17)
NOESMr1-ALADIN63 ()	1.37 (1.10 ... 1.58)	-0.070 (-0.24 ... 0.080)
NOESMr1-COSMOcrCLIM ()	1.11 (0.860 ... 1.32)	-0.17 (-0.40 ... 0.050)
NOESMr1-HADREM ()	1.34 (1.07 ... 1.57)	-0.19 (-0.35 ... -0.020)
NOESMr1-HIRHAM ()	1.43 (1.15 ... 1.66)	-0.20 (-0.37 ... 0.040)
NOESMr1-RACMO ()	1.32 (1.07 ... 1.54)	-0.13 (-0.31 ... 0.060)
NOESMr1-RCA ()	1.27 (0.810 ... 1.54)	-0.20 (-0.45 ... 0.38)
NOESMr1-REGCM ()	1.16 (0.790 ... 1.44)	0.070 (-0.24 ... 0.48)
NOESMr1-REMO ()	1.37 (1.10 ... 1.63)	-0.21 (-0.43 ... 0.0)
NOESMr1-WRF381P ()	1.50 (1.16 ... 1.80)	0.060 (-0.20 ... 0.29)
FLOR historical+RCP4.5 (5)	1.95 (1.81 ... 2.09)	-0.24 (-0.31 ... -0.18)
AM2.5C360 amip (10)	1.78 (1.68 ... 1.87)	-0.16 (-0.21 ... -0.12)
ACCESS-CM2 ssp585 (4)	1.36 (0.973 ... 1.76)	-0.12 (-0.17 ... -0.070)
ACCESS-ESM1-5 ssp585 (40)	1.89 (1.76 ... 2.02)	-0.11 (-0.13 ... -0.093)
AWI-CM-1-1-MR ssp585 (1)	1.09 (0.556 ... 1.60)	-0.29 (-0.40 ... -0.18)
CAMS-CSM1-0 ssp585 (1)	0.913 (0.0330 ... 1.75)	-0.11 (-0.20 ... -0.021)
CMCC-CM2-SR5 ssp585 (1)	1.62 (1.00 ... 2.23)	-0.063 (-0.15 ... 0.045)
CMCC-ESM2 ssp585 (1)	1.14 (0.555 ... 1.71)	-0.011 (-0.11 ... 0.12)
CNRM-CM6-1 ssp585 (1)	2.10 (1.44 ... 2.74)	-0.20 (-0.28 ... -0.10)
CNRM-CM6-1-HR ssp585 (1)	1.07 (0.328 ... 1.76)	-0.19 (-0.30 ... -0.071)

CNRM-ESM2-1 ssp585 (1)	1.76 (1.11 ... 2.37)	-0.13 (-0.23 ... -0.015)
CanESM5 ssp585 (50)	0.998 (0.942 ... 1.05)	-0.22 (-0.23 ... -0.21)
EC-Earth3 ssp585 (5)	1.03 (0.738 ... 1.30)	-0.15 (-0.19 ... -0.10)
EC-Earth3-Veg ssp585 (7)	0.756 (0.514 ... 0.997)	-0.14 (-0.18 ... -0.11)
EC-Earth3-Veg-LR ssp585 (3)	1.06 (0.594 ... 1.53)	-0.12 (-0.18 ... -0.059)
FGOALS-g3 ssp585 (3)	0.648 (0.271 ... 1.05)	-0.20 (-0.25 ... -0.15)
GFDL-CM4 ssp585 (1)	1.37 (0.646 ... 2.03)	-0.15 (-0.24 ... -0.049)
GFDL-ESM4 ssp585 (1)	0.474 (-0.460 ... 1.36)	-0.16 (-0.25 ... -0.062)
HadGEM3-GC31-LL ssp585 (4)	1.57 (1.29 ... 1.87)	-0.11 (-0.16 ... -0.062)
HadGEM3-GC31-MM ssp585 (4)	1.43 (1.07 ... 1.78)	-0.083 (-0.13 ... -0.031)
INM-CM4-8 ssp585 (1)	1.95 (0.657 ... 3.20)	-0.12 (-0.21 ... -0.015)
INM-CM5-0 ssp585 (1)	2.49 (1.22 ... 3.67)	-0.18 (-0.27 ... -0.088)
IPSL-CM6A-LR ssp585 (6)	1.43 (1.17 ... 1.68)	-0.23 (-0.26 ... -0.18)
MIROC-ES2L ssp585 (10)	1.45 (1.23 ... 1.68)	-0.21 (-0.23 ... -0.19)
MIROC6 ssp585 (50)	1.11 (1.01 ... 1.22)	-0.15 (-0.16 ... -0.14)
MPI-ESM1-2-HR ssp585 (2)	0.677 (0.189 ... 1.16)	-0.21 (-0.28 ... -0.14)
MPI-ESM1-2-LR ssp585 (30)	0.327 (0.204 ... 0.459)	-0.24 (-0.25 ... -0.22)
MRI-ESM2-0 ssp585 (6)	1.27 (0.976 ... 1.56)	-0.20 (-0.23 ... -0.17)
NorESM2-MM ssp585 (1)	2.37 (1.22 ... 3.49)	-0.23 (-0.32 ... -0.12)
TaiESM1 ssp585 (1)	1.54 (0.703 ... 2.35)	-0.10 (-0.18 ... 0.0070)
UKESM1-0-LL ssp585 (5)	1.33 (0.997 ... 1.66)	-0.089 (-0.13 ... -0.040)
CNRM-CM6-1-HR highresmip	1.678 (1.352... 1.929)	-0.094 (-0.358... 0.068)
EC-Earth3P-HR highresmip	1.558 (1.179...1.823)	-0.148 (-0.348... 0.079)
MRI-AGCM3-2-H highresmip	1.813 (1.449...2.088)	-0.001 (-0.193... 0.144)
MRI-AGCM3-2-S highresmip	1.541 (1.172...1.859)	-0.075 (-0.294... 0.151)
HadGEM3-GA6-N216 (525)	0.477 (0.378... 0.539)	-0.289 (-0.430... -0.125)

## References

*All references are hyperlinked in the main text.*